

## Complex Organics Surrounding the FU Ori-Type Object V1057 Cyg Indicative of Sublimated Ices

JENNY K. CALAHAN,<sup>1,2</sup> EDWIN A. BERGIN,<sup>1</sup> MEREL VAN'T HOFF,<sup>1</sup> ALICE BOOTH,<sup>2</sup> KARIN ÖBERG,<sup>2</sup> KE ZHANG,<sup>3</sup>  
NURIA CALVET,<sup>1</sup> AND LEE HARTMANN<sup>1</sup>

<sup>1</sup>University of Michigan, 323 West Hall, 1085 South University Avenue, Ann Arbor, MI 48109, USA

<sup>2</sup>Center for Astrophysics | Harvard & Smithsonian, 60 Garden St., Cambridge, MA 02138, USA

<sup>3</sup>Department of Astronomy, University of Wisconsin-Madison, 475 N. Charter St., Madison., WI 53706

Submitted to APJ

### ABSTRACT

FU Ori and EX Lup type objects present natural experiments for understanding a critical stage in the star and planet formation process. These objects offer insight into the diversity of molecules available to forming planetary systems due to a sudden increase in accretion and central luminosity causes the disk and surrounding material to increase in temperature. This allows for volatiles to sublimate off of grains and exist in the gas-phase for tens to hundreds of years post initial outburst. While this dynamic stage may be common for solar-type protostars, observations of the chemical impact of these bursts are rare. In this article, we present observations from the Northern Extended Millimeter Array (NOEMA) of five Young Stellar Objects (YSOs) that have undergone outbursts within the past 100 years and catalog the volatile chemistry found within  $\sim 1000$  au of the YSO. Only one source clearly shows a line rich spectra with  $>11$  molecules detected including complex organics and water, as is an expected spectra signature for a post-outburst source. This source is V1057 Cyg, and we present it as the northern analog to the well studied and molecule-rich FU Ori source, V883 Ori. Our conclusions on the chemical inventory of the other four sources in our sample are sensitivity limited, as V1057 Cyg contains the highest disk/envelope gas mass.

*Keywords:* protoplanetary disk, astrochemistry

### 1. INTRODUCTION

The majority of young stellar objects likely undergo episodic accretion events as they evolve onto the main sequence (Hartmann et al. 1997; Audard et al. 2014, i.e.). Extreme changes in luminosity were captured towards YSOs with infrared excesses as early as the 1970s (Herbig 1977). These objects would undergo sudden and intense brightening in observed magnitudes, translating to a rise in 10-100 times their original luminosity. These objects are called FU Ori-type objects (FUOrs) after their namesake source FU Ori. Two other FUOrs identified early-on are V1057 Cyg and V1515 Cyg, and since then the sample of “classic” FUOrs has expanded to  $\sim 15$  (Audard et al. 2014; Connelley & Reipurth 2018). FUOr-like objects do not have an observed increase in luminosity but have FUOr-like features in their spectra (i.e., CO absorption in the mid-IR, ‘peaky’ and rich water vapor lines, absence of emission lines; see Connelley & Reipurth 2018, for a detailed summary). After

the initial quick rise, a slow decline in luminosity takes place, taking at least 100 years for a source to reach quiescence. Each source has a different morphology in its decline in brightness over time, with some source fading quickly at first, then plateauing over time (V1057 Cyg). Others decline in brightness much more slowly (FU Ori) (Hartmann & Kenyon 1996).

EXOr outbursts are a different classification of outbursting event towards YSOs and their surrounding disk. These sources also exhibit rises in observed brightness, but the increase in their luminosity is less dramatic (factors of 2–10), and the rise and fall of their bolometric luminosity completes after a much shorter period of time ( $\sim 1$ -10 yrs). All in all, there are 40+ known eruptive young stars (see Szabó et al. 2022), with a recent increase in FUOr/EXLup candidates due to missions like Gaia and other wide-field telescopes (e.g., Tran et al. 2024; Giannini et al. 2024).

The increase in luminosity in both FUOrs and EXOrs is attributed to sudden increases in the accretion rate from the disk onto the star, with accretion rates reaching  $10^{-4}$ – $10^{-5}$   $M_{\odot}/\text{yr}$  for FUOrs (Hartmann & Kenyon 1996; Audard et al. 2014; Fischer et al. 2023). The exact mechanism that triggers FUOr outbursts is not known, however it likely involves one or more of the following: (1) a gravitationally triggered magnetorotational instability (Hartmann & Kenyon 1996; Liu et al. 2016; Cieza et al. 2018) (2) a thermal instability caused by trapped heat in high opacity regions (Bell & Lin 1994; Armitage et al. 2001; Boley et al. 2006; Zhu et al. 2010) (3) fragmentation of the disk in the outer regions and/or periodic infall from a surrounding envelope (Vorobyov & Basu 2006; Vorobyov et al. 2013; Lee et al. 2024) (4) an interaction with a near-by stellar companion or massive planet (Bonnell & Bastien 1992).

Sources identified as FUOrs have been classified as both Class I and II objects, however most likely fall between the Class I-II stage. Many (but not all) FUOrs appear to have a remaining envelope surrounding the disk itself, and are located in active star forming regions. Lying between the Class I-II phase coincides with the advent of planet formation. Looking at disk structure, disks around Class 0/I source exhibit little to no rings, gaps, or asymmetric structures (Ohashi et al. 2023) while Class II protoplanetary disks nearly always have disk substructure when seen in the continuum (Andrews et al. 2018). At least some of these substructures are presumed to be a direct or indirect result of Jupiter-mass protoplanets already coalesced within Class II protoplanetary disks, insinuating that the planet formation process starts early and happens quickly. Thus, these initial stages of planet formation very likely occur alongside energetic outburst events as is found in FUOrs. This makes these sources critical data points in gaining an understanding of both star and planet formation.

An FUOr-type outburst is a natural laboratory for revealing the chemical content of the ice reservoir within planet-forming disks, and for tracking chemical timescales. A convenient consequence of a sudden burst of accretion is that the surrounding disk will undergo a rapid increase in temperature. The volatile chemical reservoir that is typically frozen out onto the surfaces of dust grains will sublime and become a part of the more-easily-observable gas-phase population of a disk. The volatile content that is locked onto the ice mantle surrounding dust grains within roughly 10 au is the main volatile reservoir for forming planetary cores, and an outburst event offers an extremely rare opportunity to catalog this volatile planet-forming material. Thus, FUOr-type outbursts offer a glimpse into the chemistry

of forming planets. V883 Ori is the best example of this, an FUOr source that has proven to be volatile rich with tens of different molecules detected in this source alone (van ’t Hoff et al. 2018; Lee et al. 2019, 2024; Tobin et al. 2023; Yamato et al. 2024). It is thought that a source like V883 Ori is not uniquely-rich in these volatiles, but the outbursting conditions allow for typical disk chemistry to be exposed. V883 Ori has been thoroughly observed source, and as of recently, is one of the only classic FU Ori source known to be highly line-rich. L1551 IRS 5 is another FUOr-like source that appears to be rich with molecular lines (Marchand et al. 2024). HBC494 is yet another FUOr object that has been observed over a wide bandwidth with NOEMA, with some detections of  $\text{CH}_3\text{OH}$  and  $\text{CH}_3\text{CN}$ , but otherwise has a line-poor spectrum (van’t Hoff et al. 2024).

These two sources currently are the only two sources observed with high sensitivity, across a wide bandwidth, with interferometers, and these FUOrs are thought to represent ‘typical’ Class I/II sources. They provide data points for COMs, sulfur-rich species, and water; connecting the dots between bright, line-rich protostars, a few Class II protoplanetary disks, and comets. Other FUOr sources should be surveyed so that additional data can fill in this knowledge gap.

In this paper, we present a survey of five outbursting sources observed with the NOthern Extended Millimeter Array (NOEMA<sup>1</sup>). We present the chemical inventory of each source, focusing on the most molecule-rich source in our sample, and present upper limits on the non-detections for the other four sources.

## 2. METHODS

### 2.1. Source Selection

The goal of our observational survey was to identify sources that would be ideal candidates to find a chemical signature indicative of an outburst. The best candidates will be bright and massive sources, thus, we isolate objects that have been published and observed with NOEMA or the Atacama Large Millimeter Array (ALMA) in  $\text{C}^{18}\text{O}$   $J=1-0$  or  $2-1$ , and are located within the observational range of NOEMA (Fehér et al. 2017; Principe et al. 2018; Ábrahám et al. 2018). There are nine total sources that fit this criteria; we chose the brightest five sources, each with  $\text{C}^{18}\text{O}$  emission peaking directly on source. Within the northern hemisphere,

<sup>1</sup> Based on observations carried out with the IRAM Interferometer NOEMA. IRAM is supported by INSU/CNRS (France), MPG (Germany) and IGN (Spain)

**Table 1.** Source Properties

| Name      | Classification | R.A.            | Dec               | Gaia<br>Distance [pc] | Stellar Asso.<br>Distance [pc] | Outburst<br>Date | $L_{\text{bol}}$ Peak<br>[ $L_{\odot}$ ] |
|-----------|----------------|-----------------|-------------------|-----------------------|--------------------------------|------------------|--|
| V1057 Cyg | FU Ori         | 20h 58m 53.733s | +44d 15' 28.389'' | 907 $^{+19}_{-20}$    | 795                            | 1970             | 250-800                                  |
| V1735 Cyg | FU Ori         | 21h 47m 20.663s | +47d 32' 3.857''  | 691 $^{+35}_{-38}$    | 752                            | 1957-1965        | 235                                      |
| V1647 Ori | Peculiar       | 5h 46m 13.137s  | -0d 6' 4.885''    | 413 $^{+20}_{-22}$    | n/a                            | 1966, 2003, 2008 | 34-44                                    |
| V1515 Cyg | FU Ori         | 20h 23m 48.016s | +42d 12' 25.781'' | 902 $^{+12}_{-13}$    | 960                            | 1950             | 200                                      |
| V2492 Cyg | UX Ori/EX Ori  | 20h 51m 26.237s | +44d 05' 23.869'' | 804 $^{+24}_{-26}$    | n/a                            | 2009-2010        | 43                                       |

NOTE—Distances taken from parallaxes in Gaia Release 3 (Gaia Collaboration et al. 2020), however it is worth noting that outburst sources are particularly difficult to determine distances to. Other work use the assumed stellar associations to determine distances to these sources, and can disagree with GR3 by 100 parsecs (see Kuhn & Hillenbrand 2019). Outburst date and luminosity taken from review Audard et al. (2014) and references therein. Stated ranges indicate the timespan where the onset of the outburst could have started.

these objects have the highest likelihood of a optically thin mass tracers as well as molecules expected to be sublimated off of dust grains. More source information, and their properties can be found in Table 1.

### 2.2. NOEMA Observations

These results are derived from NOEMA observations that took place July - October 2021 as a part of project S21AL. Each source was observed for  $\sim 3.4$  hrs with a beam sizes  $\sim 1.''58 \times 1.''50$  (V1735 Cyg, V1057 Cyg)  $2.''45 \times 1.''69$  (V1647 Ori)  $1.''04 \times 0.''92$  (V2492 Cyg, V1515 Cyg). We used Band 3, specifically in the range of 202-211 GHz (lower sideband) and 218-226 GHz (upper sideband). This setup simultaneously covers the  $^{13}\text{CO}$ ,  $\text{C}^{18}\text{O}$ ,  $\text{C}^{17}\text{O}$ , and  $^{13}\text{C}^{18}\text{O}$  J=2-1 transitions at 2 MHz resolution. We placed high velocity windows (62.5 kHz) over a select number of lines including the CO isotopologues,  $\text{CH}_3\text{CN}$ ,  $\text{H}^{13}\text{CO}$ , HDO,  $\text{H}_2\text{CS}$ , SO, and  $\text{SO}_2$ . These lines were expected to be bright, thus line wing morphology can be probed. Further data reduction details and results from the CO isotopologues are detailed in Calahan et al. (2024).

## 3. RESULTS

### 3.1. Line Detections

In addition to CO isotopologues, all of our sources have centrally peaked emission from SO (transitions  $4_5-3_4$  and  $6_5-5_4$ ) and  $\text{H}_2\text{CO}$  (transitions  $3_{03}-2_{02}$  and  $3_{12}-2_{11}$ ). Additional lines of  $\text{H}_2\text{CO}$  and  $\text{SO}_2$  are detected with varying degree of certainty across the sample (see Table 2 and Figure 1). Beyond our expected science lines, serendipitous line detections were numerous over the large bandwidth that NOEMA offers. Using SPLATALOUGE we search for lines within this range

and identify the most likely transition to be associated with the observed line. The most likely molecule will be a molecule/transition that has already been observed, especially within the context of protoplanetary disks/FUOrs (i.e.  $\text{H}_2\text{CO}$ ,  $\text{CH}_3\text{CN}$ , HDO).  $\text{CH}_3\text{OH}$  is the most common complex organic molecule (COM) when considering the ice and gas reservoir combined, and if an ice sublimation signature was left behind in the gas,  $\text{CH}_3\text{OH}$  should be present. In three out of five of our sources, we have no detection of any  $\text{CH}_3\text{OH}$  transitions, in V2492 Cyg we have two 2-3 $\sigma$  detections of  $\text{CH}_3\text{OH}$  transitions. A few of our identified lines have only been detected in a few protoplanetary disks, but have been widely seen in protostars (SO,  $\text{SO}_2$ ,  $\text{CH}_3\text{OCHO}$ ). In this paper we only present molecular detections that have ideally multiple transitions with peak fluxes  $>4\sigma$ .

V1057 Cyg stands out in this sample as the most molecule-rich, by far (see Figure 1,2). It appears to have released the molecular complexity that is expected to reside within the ice (i.e. McClure et al. 2023), and these sublimated ices have remained in the gas perhaps since its outburst in 1970. Here, we identify bright lines that have a high signal-to-noise (all  $>3\sigma$ ), so that the line is clearly visible by-eye, and identify each transition that will be used to constrain an excitation temperature and column density (see Table A1 in appendix). In addition the aforementioned CO isotopologues, molecules that have robust,  $>>3\sigma$  detections include water (HDO), complex organic molecules (COMs:  $\text{CH}_3\text{OH}$ ,  $\text{CH}_3\text{CN}$ ,  $\text{CH}_3\text{OCHO}$ ) the building blocks for COMs ( $\text{H}_2\text{CO}$ ,  $\text{HC}_3\text{N}$ ), including an isotopologue ( $\text{H}_2^{13}\text{CO}$ ), and sulfur bearing molecules ( $\text{SO}_2$ , SO, OCS,  $\text{H}_2\text{CS}$ ).

### 3.2. Column Density & Temperature Extraction from CASSIS

**Table 2.** Identified Lines Across all Outburst Sources

| Molecule                | Transition        | Frequency (GHz) | V1057 Cyg | V1515 Cyg | V1647 Ori | V1735 Cyg | V2492 Cyg |
|-------------------------|-------------------|-----------------|-----------|-----------|-----------|-----------|-----------|
| $^{13}\text{CO}$        | J=2-1             | 220.399         | ✓         | ✓         | ✓         | ✓         | ✓         |
| $\text{C}^{18}\text{O}$ | J=2-1             | 219.560         | ✓         | ✓         | ✓         | ✓         | ✓         |
| $\text{C}^{17}\text{O}$ | J=2-1             | 224.714         | ✓         | ✓         | ✓         | ✓         | ✓         |
| SO                      | 4(5)-3(4)         | 206.176         | ✓         | ✓         | ✓         | ✓         | ✓         |
| SO                      | 6(5)-5(4)         | 219.949         | ✓         | ✓         | ✓         | ✓         | ✓         |
| SO <sub>2</sub>         | 12(0,12)-11(1,11) | 203.392         | ✓         | *         | ✗         | ✗         | ✗         |
| SO <sub>2</sub>         | 11(2,10)-11(1,11) | 205.301         | ✓         | ✗         | ✗         | *         | ✗         |
| H <sub>2</sub> CO       | 3(0,3)-2(0,2)     | 218.222         | ✓         | ✓         | ✓         | ✓         | ✓         |
| H <sub>2</sub> CO       | 3(1,2)-2(1,1)     | 225.698         | ✓         | ✓         | ✓         | ✓         | ✓         |
| H <sub>2</sub> CO       | 3(2,2)-2(2,1)     | 218.476         | ✓         | ✗         | ✗         | *         | ✓         |
| H <sub>2</sub> CO       | 3(2,1)-2(2,0)     | 218.760         | ✓         | ✗         | ✗         | ✓         | *         |

NOTE—All of the above molecules and transitions have a bright detection in source V1057 Cyg and across all other sources, either have a bright detection ( $>3\sigma$ , denoted by ✓), a tentative detection ( $\approx 3\sigma$ , \*), or no detection (✗). Every other transition found in V1057 Cyg (Table A1) is not detected in any other source.

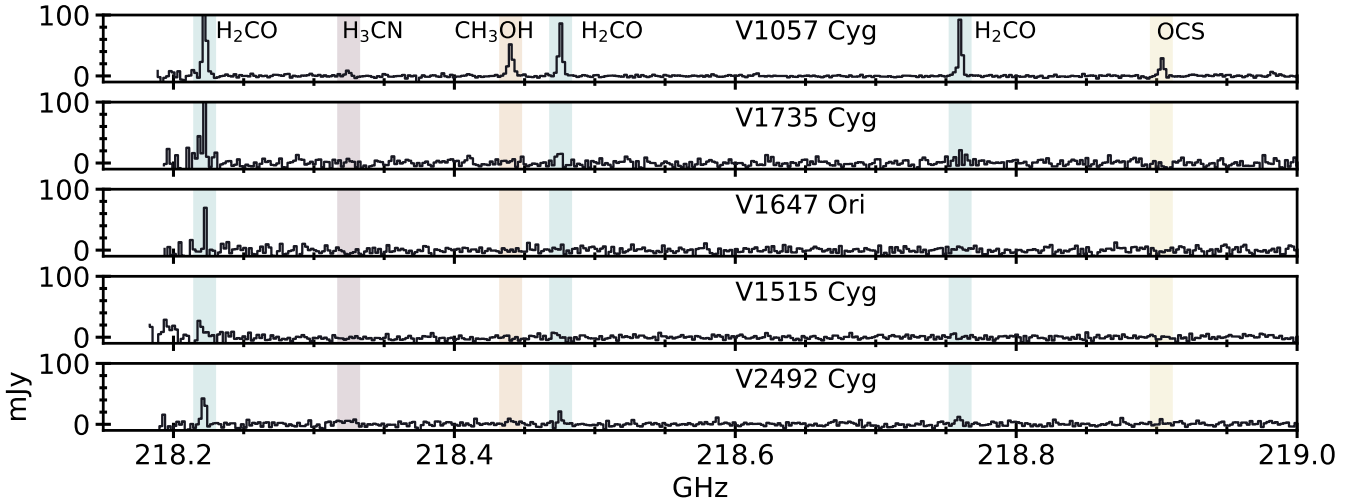


**Figure 1.** An example of the spectra of the central pixel of each source between 218.2-219 GHz. This region shows how V1057 Cyg is markedly more line-rich than each of the other sources.

We use CASSIS<sup>2</sup> (Vastel et al. 2015) which is a slab modeling tool for spectral analysis to determine column densities and excitation temperatures for the molecules detected in V1057 Cyg. We assumed LTE and utilized the line lists from the JPL line catalogue<sup>3</sup>. For each of the molecules with three or more transitions, we perform a grid exploration of column density, tem-

perature, and full-width half-max (FWHM) of the line. For each line we explore column densities between  $10^{13}$  and  $10^{18}$   $\text{cm}^{-2}$ , excitation temperatures between 40 and 300 K, and FWHM between 3 and 7 km/s. We include lines in our slab models for any transition that has an  $A_{ij}$  greater than  $10^{-6}$  and all transitions with an  $E_{up}$  lower than 500 K, so that both line detections and non-detections can constrain our final column density and temperature. A  $\chi^2$  fitting routine was done to determine the slab model within the explored parameter space that fit the data best. Both line detections and non-detections were used to constrain a column density

<sup>2</sup> <http://cassis.irap.omp.eu>

<sup>3</sup> <https://spec.jpl.nasa.gov/home.html>

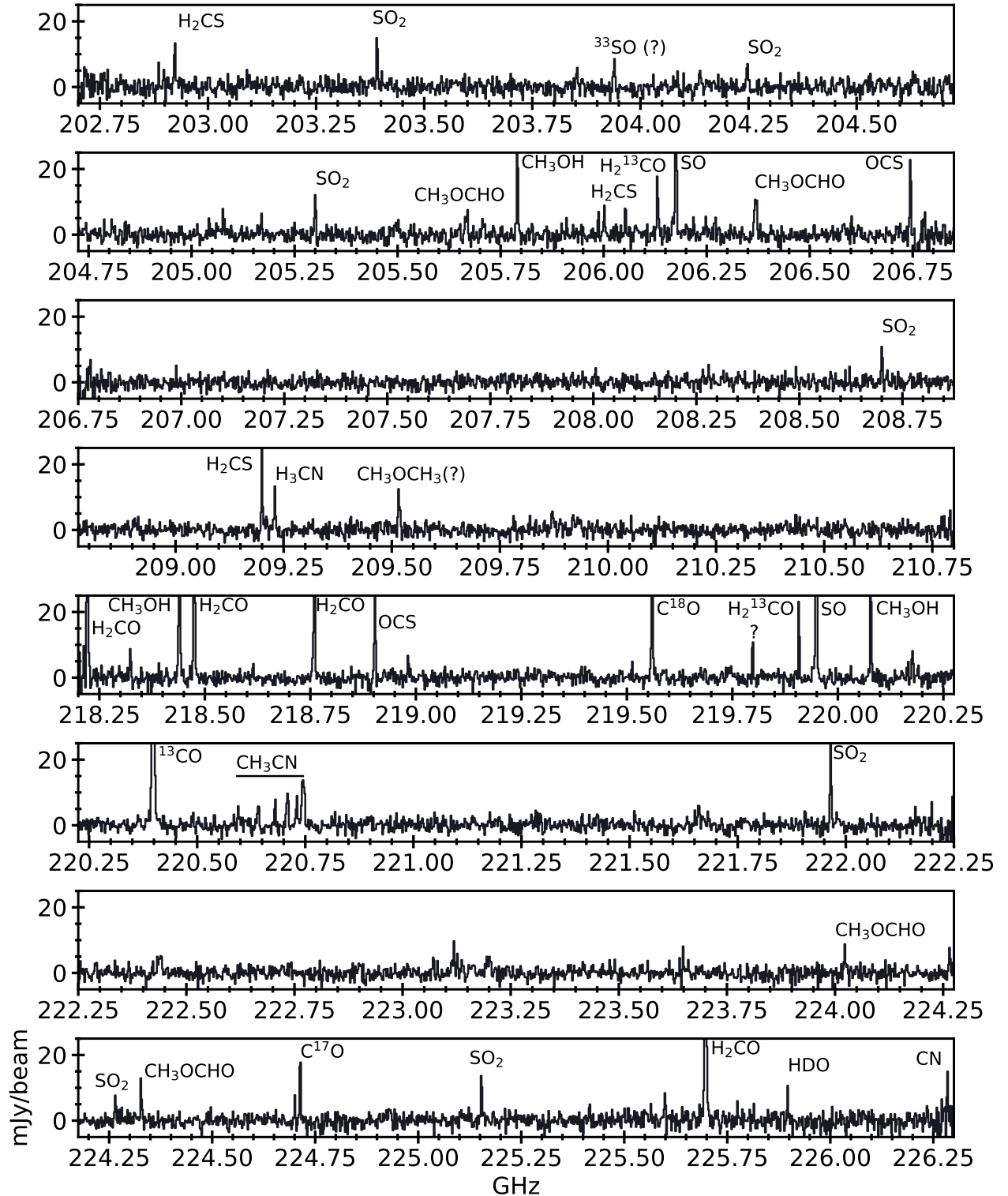


**Figure 2.** The full lower and upper sideband coverage of V1057 Cyg. Lines that are used to calculate column densities or mass are highlighted. Lines identified with a "?" are tentative detections, mostly due to only one transition identified and it being a rare molecule to detect in protoplanetary disks.



**Table 3.** Column Densities for Detected Molecular Species in V1057 Cyg

| Molecule                         | $T_{ex}$<br>[K]  | Column Density<br>[ mol/cm <sup>2</sup> ] |
|----------------------------------|------------------|---|
| Sulfur Species                   |                  |   |
| SO <sub>2</sub>                  | 80               | $1.6(\pm 0.32)\times 10^{14}$             |
| H <sub>2</sub> CS                | 80               | $4.0(\pm 0.80)\times 10^{13}$             |
| SO                               | 120 <sup>a</sup> | $2.5(\pm 0.50)\times 10^{14}$             |
| OCS                              | 80 <sup>a</sup>  | $1.6(\pm 0.32)\times 10^{14}$             |
| Building-block COMs              |                  |   |
| CH <sub>3</sub> CN               | 110              | $1.0(\pm 0.20)\times 10^{13}$             |
| H <sub>2</sub> CO                | 90               | $2.5(\pm 0.50)\times 10^{14}$             |
| CH <sub>3</sub> OH               | 180              | $3.2(\pm 0.64)\times 10^{15}$             |
| H <sub>3</sub> CN                | 120 <sup>a</sup> | $2.5(\pm 0.50)\times 10^{14}$             |
| H <sub>2</sub> <sup>13</sup> CO  | 80 <sup>a</sup>  | $1.6(\pm 0.32)\times 10^{13}$             |
| H <sub>2</sub> C <sup>17</sup> O | 80 <sup>a</sup>  | $1.6(\pm 0.32)\times 10^{13}$             |
| Long COMs                        |                  |   |
| CH <sub>3</sub> OCHO             | 120              | $2.5(0.5)\times 10^{14}$                  |
| Water                            |                  |   |
| HDO                              | N/A              | $2.0(0.40)\times 10^{14}$                 |

NOTE— Column density and temperature with the lowest  $\chi^2$  are reported.  $2\sigma$  errors derived from the  $\chi^2$  minimization given a fixed temperature gave column density uncertainties less than 20%, which is believed to be less than the calibration uncertainty, thus 20% errors are stated. <sup>a</sup>These molecules had 1-2 strong transitions and the temperatures 80, 120, and 180 K were used to determine a column density. Out of these models, the one with the lowest  $\chi^2$  is reported in this table.

and temperature for each molecule that had three or more transitions. Temperature is not well constrained, between the explored range solutions within a  $1\sigma$  certainty exist, given a fixed temperature however the column densities can be constrained. To calculate our errors, we fix our slab model to the 40 and 300 K and determine the lowest and highest column density within a  $1\sigma$  certainty, respectively. In V1057 Cyg, molecules with three or more transitions were CH<sub>3</sub>OH, H<sub>2</sub>CO, SO<sub>2</sub>, CH<sub>3</sub>CN, H<sub>2</sub>CS, and CH<sub>3</sub>OCHO. The final column densities and temperatures from the slab model with the smallest  $\chi^2$  are shown in Table 3.

The rest of our detected molecules have 1-2 transitions, which would not provide enough strong constraints on a parameter exploration to determine their

column densities and excitation temperatures. Thus, we choose to keep the temperature fixed, and iterate over the same column density range as before. We do this  $\chi^2$  minimization over three different fixed temperatures (80 K, 120 K, 160 K), motivated by the temperatures found for molecules with 3+ transitions. For each temperature and column density combination we calculate the  $\chi^2$ , and report back the temperature and column density that has the lowest overall  $\chi^2$  value. One line of HDO is not enough to put a constraint on temperature, but across 80, 120, and 180 K a column density of  $1.0\times 10^{14}$  (cm<sup>-2</sup>) returned the lowest  $\chi^2$ . The fact that these molecules are detected at relatively high abundances, and at temperatures above their sublimation temperature points to these volatiles being sublimated off of grains.

We also calculate upper limits on the CH<sub>3</sub>OH column density for each source that has non-detections of any CH<sub>3</sub>OH lines. LTE slab models are created using the derived excitation temperature from V1057 Cyg (180 K). A series of column densities are used, and when a slab model with a certain column density creates a line that should have been detected at the  $3\sigma$  level, we use that as our upper limit for the CH<sub>3</sub>OH. To provide context to the derived methanol column density, we also derive C<sup>17</sup>O and H<sub>2</sub>CO column densities. H<sub>2</sub>CO has two or more strong detections in each of our sources, thus we use a  $\chi^2$  fitting technique. More on calculating the column density, and the optically thin emission from C<sup>17</sup>O as a mass tracer can be found in Calahan et al. (2024).

## 4. ANALYSIS & DISCUSSION

### 4.1. Line Accounting

Beyond the CO lines, at least two bright formaldehyde transitions are detected ubiquitously across the sample. H<sub>2</sub>CO detections are not particularly surprising, as this is a common molecule found within both protoplanetary disks and earlier Class 0/I sources (i.e. Pegues et al. 2020; Jørgensen et al. 2007). H<sub>2</sub>CO emission is associated with warm gas and shocks, and seems to be present in disk environments over a wide range of gas masses. Ubiquitous detections of SO and tentative detections of SO<sub>2</sub> in three of our sources however, is surprising. SO and SO<sub>2</sub> are have been found in only four quiescent Class II protoplanetary disks - all massive disks around Herbig Ae/Be stars (Rivière-Marichalar et al. 2020; Booth et al. 2021; Law et al. 2023; Booth et al. 2023). Sulfur-bearing molecules are found more often within protostars, however the explanation for its origin can come from shocks or infall, releasing these molecules from ice grains (i.e.

**Table 4.** Column Densities and Mass Across Sample

| Molecule                            | V1057 Cyg            | V2492 Cyg            | V1735 Cyg              | V1515 Cyg                 | V1647 Ori                 |
|-------------------------------------|----------------------|----------------------|------------------------|---------------------------|---------------------------|
| CH <sub>3</sub> OH                  | $3.2 \times 10^{15}$ | $1.0 \times 10^{15}$ | $< 1.5 \times 10^{15}$ | $< 1.0 \times 10^{15}$    | $< 5.0 \times 10^{14}$    |
| H <sub>2</sub> CO                   | $2.5 \times 10^{14}$ | $2.5 \times 10^{14}$ | $6.30 \times 10^{13}$  | $\sim 6.3 \times 10^{13}$ | $\sim 2.5 \times 10^{13}$ |
| C <sup>17</sup> O                   | $2.0 \times 10^{17}$ | $7.0 \times 10^{17}$ | $1.9 \times 10^{16}$   | $5.5 \times 10^{16}$      | $1.5 \times 10^{17}$      |
| Inner Region Mass [M <sub>⊙</sub> ] | 3.4                  | 1.9                  | 0.25                   | 0.58                      | 0.42                      |

NOTE—Derived column densities or upper limits for each source (mol/cm<sup>2</sup>); see Figure 3. The derivation for inner region mass including envelope and disk emission can be found in Calahan et al. (2024)

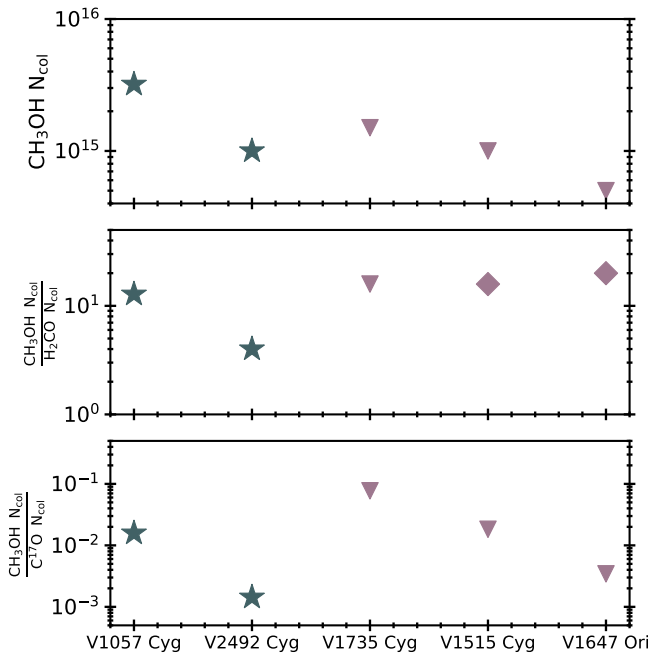


**Figure 3.** Column densities of CH<sub>3</sub>OH in V1057 Cyg (based on 5 transitions) and V2492 Cyg (based on two transitions) and derived upper limits from the non-detections towards the three other sources (top). The ratio between the CH<sub>3</sub>OH column density or upper limit and a derived H<sub>2</sub>CO column density (middle) and C<sup>17</sup>O column density (bottom). Points with stars indicate that detected line(s) are used to determine the column density. A triangle indicates an upper limit, and diamond utilized both an upper limit on the methanol and a H<sub>2</sub>CO column density based on just two transitions.

Artur de la Villarmois et al. 2019; Le Gal et al. 2020). In our outburst sources, SO (and SO<sub>2</sub>) detections are bright and centrally peaked with only a mild asymmetry in the line wings. This suggests that the majority of the sulfur was released from ices within the disk for each of our sources, as opposed to fast moving shocked gas at a very different velocity than the source. The presence of SO can come from the outburst event, leaving a sublimated ice-signature behind or it has also been shown

that SO and H<sub>2</sub>CO can be enhanced in gravitationally unstable disks, due to heat from spiral structure and shocks (Evans et al. 2015, 2019).

Four of our sources (V1515 Cyg, V1735 Cyg, V1647 Ori, and V2492 Cyg) are void of bright lines outside of CO isotopologues, H<sub>2</sub>CO, SO, and tentatively SO<sub>2</sub>. Notably, none of them exhibit strong lines of the most common COM - CH<sub>3</sub>OH. In order to determine if the reason behind the CH<sub>3</sub>OH detection in V1057 Cyg comes from its high mass, or something unique about this system we determine upper limits on the CH<sub>3</sub>OH column density for our other sources. The upper limits on CH<sub>3</sub>OH are shown in Figure 3. For V2492 Cyg, we have two 2-3 $\sigma$  detected transitions of CH<sub>3</sub>OH thus we run slab models to determine if 80, 120, or 180 K provide the best fit to the data. We find that we get the best model with an excitation temperature of 120 K and a column of  $1 \times 10^{15}$  cm<sup>-2</sup>, about a factor of three less than what was found in V1057 Cyg. All other methanol column density upper limits are also determined to be lower than V1057 Cyg.

#### 4.2. An Apparent Dichotomy in Chemical Signatures

When comparing spectral data from V1057 Cyg to our other sources, V1057 Cyg appears to have a markedly different chemistry. The chemical richness is representative of what we expect from ice sublimation shortly after an outburst. The fact that it is the only source in our sample that appear to have this chemical signature was not expected based on the  $\sim$ two outbursting sources that have been observed previously, V883 Ori and L1551 IRS5. The fact that four of our sources are not line-rich brings up the question as to whether there is something unique about the outburst or disk environment in V1057 Cyg that keeps this chemical signature around for 50+ years, while other sources may lose this expected chemical signatures more rapidly.

From C<sup>17</sup>O observations, V1057 Cyg is the most massive in our sample, and the mass derived from optically thin C<sup>17</sup>O is markedly higher than what would be de-

rived from continuum emission. This, in addition to a lack of clear disk features on the  $\sim 1000$ s of au scales in position-velocity space, suggests that V1057 Cyg has a significant envelope contribution, implying that V1057 Cyg may be closer to a Class I object (although previous work has identified it as a Class II source based on the SED). Adding to this source’s complexity, it is also a binary system, as seen from two peaks in the continuum observations (Calahan et al. 2024) and as was first spatially resolved by Green et al. (2016). The molecular emission from all non-CO lines appear as unresolved emission, peaked on the central star. Thus, we expect these molecular detections to be solely coming from the central protostar’s disk/envelope.

When comparing the  $\text{CH}_3\text{OH}$  column density in V1057 Cyg to our other four sources, it is 2-3 times larger than our upper limits. To provide context to the  $\text{CH}_3\text{OH}$  column, we take the ratio between  $\text{CH}_3\text{OH}$  and the one other organic that is found in all of our sources,  $\text{H}_2\text{CO}$  as well as the optically thin gas mass tracer  $\text{C}^{17}\text{O}$  (see Fig. 3). Now, we see that the  $\text{CH}_3\text{OH}$  in the other sources are comparable to V1057 Cyg or below. The limits on the other sources show that there is not a significantly higher ratio of  $\text{CH}_3\text{OH}/\text{H}_2\text{CO}$ . Compared to the one other source with tentative  $\text{CH}_3\text{OH}$  detections, V2492 Cyg, V1057 Cyg does appear to have significantly more  $\text{CH}_3\text{OH}$ , even within the context provided by  $\text{H}_2\text{CO}$ . Deeper observations of bright  $\text{CH}_3\text{OH}$  lines or in a frequency range with optically thinner dust would be required to determine if there is a clear dichotomy in the chemical signatures across FU Ori sources. Considering  $\text{CH}_3\text{OH}/\text{C}^{17}\text{O}$ , it does appear that the upper limit found in V1647 Ori is significantly lower than in V1057 Cyg, while the other two sources place the upper limit of  $\text{CH}_3\text{OH}/\text{C}^{17}\text{O}$  on order of V1057 or higher. This data set alone cannot definitively prove that V1057 Cyg has a unique chemical signatures amongst outbursting sources, its apparent molecular complexity may be due to its high gas mass within the surrounding  $\sim 1000$  au. It is peculiar that the source with the third highest gas mass and comparable dust mass (V1647 Ori) has no  $\text{CH}_3\text{OH}$  and only two detections of  $\text{H}_2\text{CO}$ . To say anything definitive about the gaseous inventory of V1735 Cyg and V1515 Cyg will require deeper observations.

#### 4.3. Complex Organic Content Evolution: Protostars to Comets

Chemical inheritance from cloud to comet is essential to constrain the critical factors that influence final planetary compositions. The chemical inventory within V1057 Cyg is rich enough to compare to pro-

tostars, other outbursting sources, protoplanetary disk, and comet data across multiple molecules (see Figure 4).

The PILS Survey is an example of the most well studied protostellar system, as it targeted the protostar IRAS 16293-2422 across a wide spectral range. This system is a binary, and both protostars appear to be quite line-rich with HDO, complex organic molecules, and sulfur-bearing species. Compared to V1057 Cyg alone, the molecular ratio between each of these molecules and  $\text{CH}_3\text{OH}$  is lower than V1057 Cyg, with the exception of  $\text{CH}_3\text{CN}$  in IRAS 16293-2422A (Persson et al. 2013; Calcutt et al. 2018; Jørgensen et al. 2018; Drozdovskaya et al. 2018; Manigand et al. 2020).

There are two other outbursting sources that have been classified as an FU Ori type object or FUOr-like and have been seen to be line-rich, which are V883 Ori and L1551 IRS 5 respectively. Based on the relative amount of envelope in each source and historical SED classifications, L1551 IRS 5 likely is the youngest out of these three, followed by V1057 Cyg, then V883 Ori. It is worth noting that between the sources that have some long-term lightcurve data, they have different trends over time. V883 Ori likely went into outburst before 1888 based on photometric plate data (Pickering 1890), and since its discovery has remained very luminous (Dent et al. 1998; Greene et al. 2008). V1057 Cyg’s outburst, however was captured as a sharp and quick rise, while then decreasingly fairly quickly at first, and then slowly yet steadily till present day (Szabó et al. 2021). Both of these sources have existed post-outburst for  $\sim 100$ -200 years, which is much shorter than a typical freeze-out time (1000+ years Visser et al. 2015). Thus even though these sources have markedly different histories, the fact that they have been post outburst within the past  $\sim 100$  years leads us to assume that the chemistry between the sources has not had time to be altered significantly. HDO appears to be by far the most abundant in V1057 Cyg, with the ratio of  $\text{HDO}/\text{CH}_3\text{OH}$  nearly two orders of magnitude higher than in L1551 IRS 5 and V883 Ori. For the sulfur-bearing species, V1057 Cyg and V883 Ori are on par with each other, and both the OCS and  $\text{SO}_2$  to  $\text{CH}_3\text{OH}$  ratios are similar. L1551 IRS 5 has a much smaller relative abundance of sulfur-bearing molecules. The COMs  $\text{CH}_3\text{CN}$  and  $\text{CH}_3\text{OCHO}$  are detected in V1057 Cyg and V883 Ori, with  $\text{CH}_3\text{OCHO}/\text{CH}_3\text{OH}$  being very similar and  $\text{CH}_3\text{CN}/\text{CH}_3\text{OH}$  just under an order of magnitude (Tobin et al. 2023; Andreu et al. 2023; Yamato et al. 2024; Marchand et al. 2024). The other FUOr object that has been targeted with NOEMA, HBC494, has a measured ratio between  $\text{CH}_3\text{CN}$  and  $\text{CH}_3\text{OH}$ , which is a factor of ten higher than what is found in V1057 Cyg.



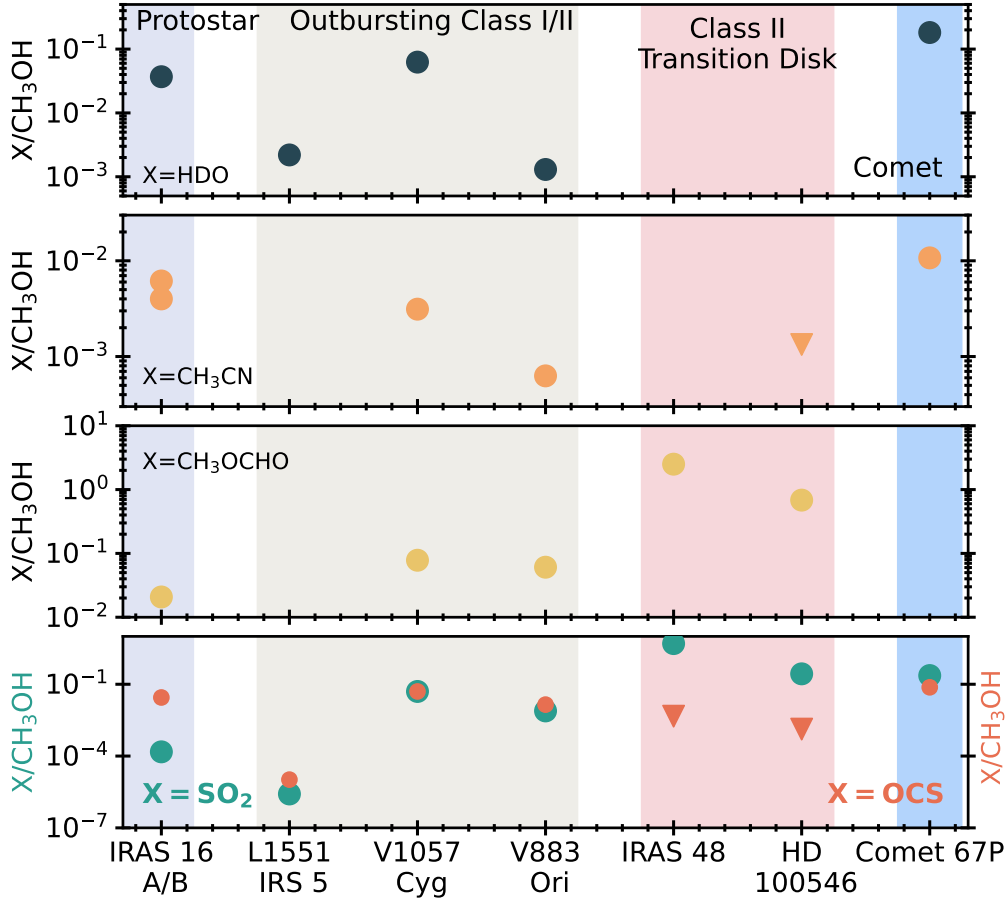


**Figure 4.** Column density ratios across protostars, outbursting sources, a protoplanetary disk, and abundance ratio from a comet of molecules with respect to  $\text{CH}_3\text{OH}$ . IRAS 16293-2422 is a binary system and both A and B are plotted along the same x-value.

Gas-rich protoplanetary disks around T Tauri stars will have a very small emitting area and gas column in which sublimated COMs, HDO, and sulfur-bearing molecules can be observed. Transitions disks around Herbig Ae/Be stars, however, offer a larger emitting area due to both the inner radius location and higher temperature. With the addition of typically higher gas masses, these objects offer the best insight into the chemistry available during the Class II stage of a protoplanetary disk. IRS 48 and HD 100546 are two transition disks which have been well studied and column densities of these sublimated molecules can be studied. In both HD 100456 and IRS 48, there are no detected  $\text{CH}_3\text{CN}$  and observations were not sensitive to HDO. Compared to the protostar and FU Ori sources, the protoplanetary disks have much higher relative abundances of the long

COM  $\text{CH}_3\text{OCHO}$  and  $\text{SO}_2$ , while the upper limit on OCS is on par with the slightly more evolved FUOrs (Booth et al. 2024a,b).

Finally, Comet 67P/Churyumov-Gerasimenko has direct detections of water,  $\text{CH}_3\text{CN}$ , OCS, and  $\text{SO}_2$ . The sulfur bearing species are on par with the FUOrs, water is slightly higher than V1057 Cyg, but significantly higher than the other FUOrs and protostar.  $\text{CH}_3\text{CN}$  in the comet is most abundant with respect to  $\text{CH}_3\text{OH}$  as compared to all other sources in this comparison (Le Roy et al. 2015; Altwegg et al. 2017; Rubin et al. 2019).

V1057 Cyg adds a critical data point between protostars, protoplanetary disks and comets. Given the limited data points, there appears to be a possible trend in the sulfur-bearing molecules and  $\text{CH}_3\text{OCHO}$ , as they increase in relative abundance across stellar age. If true,

this would suggest that large COMs and simple sulfur bearing molecules build up over time from protostar to comet. HDO and CH<sub>3</sub>CN show no clear trend. HDO especially shows a wide range in relative abundance to CH<sub>3</sub>OH, spanning across two orders of magnitude within the outbursting Class I/II sources alone. This > order of magnitude range in the HDO/CH<sub>3</sub>OH ratio is striking, and could be from optically thick CH<sub>3</sub>OH, an enhanced water or depleted CH<sub>3</sub>OH reservoir, or an enhanced D/H in water or a combination of these. Observations of isotopes of CH<sub>3</sub>OH and of H<sub>2</sub><sup>18</sup>O would shed light into which of these is most likely. More data points and wider spectral surveys of multiple line-rich objects are necessary to understand if these relative abundance trends hold, and how they may impact the chemistry available to forming planets over time.

## 5. CONCLUSION

Using NOEMA, we targeted 5 FUOr and EX Lup type sources between 202.7-210.8 GHz and 218.2-226.3 GHz. All of our sources contained emission from <sup>13</sup>CO, C<sup>18</sup>O, C<sup>17</sup>O, SO, and H<sub>2</sub>CO. One of our sources, V1057 Cyg, has a markedly different spectra, rich with volatiles that one would expect to see post-outburst when the ice has sublimated. This is akin to another FUOr, V883 Ori. This survey more than doubles the number of FUOr outburst objects that have been surveyed across a wide spectral range, yet less than half exhibit the assumed chemical signature of an outburst: V1057 Cyg, V883 Ori, and L1551. We explored whether these observed differences could be explained by differences in gas mass within the beam, and find that they could. Deeper ob-

servations are needed to investigate the range of ice compositions present in planet forming disks around young stars. In these four other sources in our sample, the molecular richness from sublimated ices could have frozen back onto grains quickly, or our observations did not go deep enough to obtain the sensitivity required. V1057 Cyg, V883 Ori, and L1551 have envelope emission, signifying that these are younger sources than other FU Or/Ex Lup objects and this could be a factor in determining the abundance of volatile-rich gas. Both sources have peak luminosities of > 200L<sub>⊙</sub> suggesting a larger area of sublimated species, however classic FUOrs V1515 Cyg and V1735 Cyg in our sample have comparably bright peak luminosities (see Table 1). More observations of outbursting sources will offer a unique glimpse into the chemistry available to forming planets, and deeper observations would greatly benefit our understanding of chemical inheritance.

## 6. ACKNOWLEDGMENTS

Matplotlib (Hunter 2007), Astropy (Astropy Collaboration et al. 2013, 2018), NumPy (Harris et al. 2020)

J.K.C. acknowledges support from the National Science Foundation Graduate Research Fellowship under Grant No. DGE 1256260 and the National Aeronautics and Space Administration FINESST grant, under Grant no. 80NSSC19K1534.

A. S. B. is supported by a Clay Postdoctoral Fellowship from the Smithsonian Astrophysical Observatory.

E.A.B. acknowledge support from NSF Grant#1907653 and NASA grant XRP 80NSSC20K0259

## APPENDIX

## REFERENCES

- Ábrahám, P., Kóspál, Á., Kun, M., et al. 2018, *ApJ*, 853, 28, doi: [10.3847/1538-4357/aaa242](https://doi.org/10.3847/1538-4357/aaa242)
- Altwegg, K., Balsiger, H., Berthelier, J. J., et al. 2017, *MNRAS*, 469, S130, doi: [10.1093/mnras/stx1415](https://doi.org/10.1093/mnras/stx1415)
- Andreu, A., Coutens, A., Cruz-Sáenz de Miera, F., et al. 2023, *A&A*, 677, L17, doi: [10.1051/0004-6361/202347484](https://doi.org/10.1051/0004-6361/202347484)
- Andrews, S. M., Huang, J., Pérez, L. M., et al. 2018, *ApJL*, 869, L41, doi: [10.3847/2041-8213/aaf741](https://doi.org/10.3847/2041-8213/aaf741)
- Armitage, P. J., Livio, M., & Pringle, J. E. 2001, *MNRAS*, 324, 705, doi: [10.1046/j.1365-8711.2001.04356.x](https://doi.org/10.1046/j.1365-8711.2001.04356.x)
- Artur de la Villarmois, E., Jørgensen, J. K., Kristensen, L. E., et al. 2019, *A&A*, 626, A71, doi: [10.1051/0004-6361/201834877](https://doi.org/10.1051/0004-6361/201834877)
- Astropy Collaboration, Robitaille, T. P., Tollerud, E. J., et al. 2013, *A&A*, 558, A33, doi: [10.1051/0004-6361/201322068](https://doi.org/10.1051/0004-6361/201322068)
- Astropy Collaboration, Price-Whelan, A. M., Sipőcz, B. M., et al. 2018, *AJ*, 156, 123, doi: [10.3847/1538-3881/aabc4f](https://doi.org/10.3847/1538-3881/aabc4f)
- Audard, M., Ábrahám, P., Dunham, M. M., et al. 2014, in *Protostars and Planets VI*, ed. H. Beuther, R. S. Klessen, C. P. Dullemond, & T. Henning, 387, doi: [10.2458/azu\\_uapress\\_9780816531240-ch017](https://doi.org/10.2458/azu_uapress_9780816531240-ch017)

**Table A1.** Molecular Transitions In V1057 Cyg Used for Slab Models Excluding CO Isotopologues

| Molecule                        | Transition         | Frequency (GHz) | $\log_{10}A_{ij}$ | $E_{up}$ (K) | V1057 Cyg Detection? |
|---------------------------------|--------------------|-----------------|-------------------|--------------|----------------------|
| CH <sub>3</sub> OH              | 12(5)-13(4)        | 206.001         | -4.98             | 317          | yes                  |
|                                 | 1(1,1)-2(0,2)++    | 205.791         | -4.473            | 16.8         | yes                  |
|                                 | 19(1)-19(0)        | 209.518         | -4.500            | 462          | yes                  |
|                                 | 4(2,2)-3(1,2)      | 218.44          | -4.329            | 45.5         | yes                  |
|                                 | 8(0,8)-7(1,6)      | 220.078         | -4.599            | 96.6         | yes                  |
|                                 | 10(5,6)-11(4,8)    | 220.401         | -4.950            | 252          | yes                  |
| H <sub>2</sub> CO               | 3(0,3)-2(0,2)      | 218.222         | -3.550            | 21.0         | yes                  |
|                                 | 3(2,2)-2(2,1)      | 218.475         | -3.595            | 68.1         | yes                  |
|                                 | 3(2,1)-2(2,0)      | 218.76          | -3.802            | 68.1         | yes                  |
|                                 | 3(1,2)-2(1,1)      | 225.697         | -3.557            | 33.5         | yes                  |
| CH <sub>3</sub> CN              | 12(0)-11(0)        | 220.747         | -2.180            | 68.9         | yes                  |
|                                 | 12(1)-11(1)        | 220.743         | -2.193            | 76.0         | yes                  |
|                                 | 12(2)-11(2)        | 220.73          | -2.234            | 97.4         | yes                  |
|                                 | 12(3)-11(3)        | 220.709         | -2.000            | 133          | yes                  |
|                                 | 12(4)-11(4)        | 220.679         | -2.397            | 183          | yes                  |
|                                 | 12(5)-11(5)        | 220.641         | -2.522            | 247          | yes                  |
|                                 | 12(6)-11(6)        | 220.594         | -2.377            | 326          | tentative            |
| SO <sub>2</sub>                 | 12(0,12)-11(1,11)  | 203.391         | -4.055            | 70.0         | yes                  |
|                                 | 18(3,15)-18(2,16)  | 204.246         | -4.033            | 181          | yes                  |
|                                 | 7(4,4)-8(3,5)      | 204.384         | -4.953            | 65.0         | tentative            |
|                                 | 11(2,10)-11(1,11)  | 205.301         | -4.270            | 70.2         | yes                  |
|                                 | 3(2,2)-2(1,1)      | 208.700         | -4.173            | 15.3         | yes                  |
|                                 | 12(5,7)-13(4,10)   | 209.936         | -4.797            | 133          | tentative            |
|                                 | 22(7,15)-23(6,18)  | 219.276         | -4.671            | 352          | no                   |
|                                 | 11(1,11)-10(0,10)  | 221.965         | -3.943            | 60.4         | yes                  |
|                                 | 6(4,2)-7(3,5)      | 223.883         | -4.935            | 58.6         | no                   |
|                                 | 20(2,18)-19(3,17)  | 224.264         | -4.400            | 207          | yes                  |
| H <sub>2</sub> CS               | 13(2,12)-13(1,13)  | 225.154         | -3.283            | 57.1         | yes                  |
|                                 | 6(1,6)-5(1,5)      | 202.923         | -3.926            | 47.3         | yes                  |
|                                 | 6(5,1)-5(5,0)      | 205.942         | -4.410            | 361          | no                   |
|                                 | 6( 0, 6)- 5( 0, 5) | 205.987         | -3.894            | 34.6         | yes                  |
|                                 | 6( 4, 3)- 5( 4, 2) | 206.001         | -4.150            | 245          | no                   |
|                                 | 6( 4, 2)- 5( 4, 1) | 206.001         | -4.150            | 245          | no                   |
|                                 | 6( 3, 4)- 5( 3, 3) | 206.051         | -4.019            | 153          | yes, blended         |
|                                 | 6( 3, 3)- 5( 3, 2) | 206.052         | -4.019            | 153          | yes, blended         |
|                                 | 6( 2, 5)- 5( 2, 4) | 206.053         | -3.945            | 87.3         | yes, blended         |
|                                 | 6( 2, 4)- 5( 2, 3) | 206.158         | -3.945            | 87.3         | no                   |
| 6( 1, 5)- 5( 1, 4)              | 209.200            | -3.886          | 48.3              | yes          |                      |
| Molecules with 1-2 Transitions  |                    |                 |                   |              |                      |
| SO                              | 4(5)- 3(4)         | 206.176         | -3.987            | 38.6         | yes                  |
|                                 | 6(5)-5(4)          | 219.949         | -3.865            | 35.0         | yes                  |
| OCS                             | 17-16              | 206.745         | -4.592            | 89.3         | yes                  |
|                                 | 18-17              | 218.903         | -4.517            | 99.81        | yes                  |
| H <sub>3</sub> CN               | 23-22              | 209.23          | -3.14             | 121          | yes                  |
|                                 | 24-23              | 218.325         | -3.084            | 130.982      | yes                  |
| H <sub>2</sub> <sup>13</sup> CO | 3( 1, 3)- 2( 1, 2) | 206.132         | -3.675            | 31.6         | yes                  |
|                                 | 3(1,2)-2(1,1)      | 219.908         | -3.591            | 32.9         | yes                  |
| HDO                             | 3(1,2)-2(2,1)      | 225.896         | -4.879            | 168          | yes                  |

- Bell, K. R., & Lin, D. N. C. 1994, *ApJ*, 427, 987, doi: [10.1086/174206](https://doi.org/10.1086/174206)
- Boley, A. C., Mejía, A. C., Durisen, R. H., et al. 2006, *ApJ*, 651, 517, doi: [10.1086/507478](https://doi.org/10.1086/507478)
- Bonnell, I., & Bastien, P. 1992, *ApJL*, 401, L31, doi: [10.1086/186663](https://doi.org/10.1086/186663)
- Booth, A. S., Ilee, J. D., Walsh, C., et al. 2023, *A&A*, 669, A53, doi: [10.1051/0004-6361/202244472](https://doi.org/10.1051/0004-6361/202244472)
- Booth, A. S., van der Marel, N., Leemker, M., van Dishoeck, E. F., & Ohashi, S. 2021, *A&A*, 651, L6, doi: [10.1051/0004-6361/202141057](https://doi.org/10.1051/0004-6361/202141057)
- Booth, A. S., Temmink, M., van Dishoeck, E. F., et al. 2024a, *AJ*, 167, 165, doi: [10.3847/1538-3881/ad26ff](https://doi.org/10.3847/1538-3881/ad26ff)
- Booth, A. S., Leemker, M., van Dishoeck, E. F., et al. 2024b, *AJ*, 167, 164, doi: [10.3847/1538-3881/ad2700](https://doi.org/10.3847/1538-3881/ad2700)
- Calahan, J. K., Bergin, E. A., van't Hoff, M., et al. 2024, *ApJ*, 967, 158, doi: [10.3847/1538-4357/ad4a5a](https://doi.org/10.3847/1538-4357/ad4a5a)
- Calcutt, H., Jørgensen, J. K., Müller, H. S. P., et al. 2018, *A&A*, 616, A90, doi: [10.1051/0004-6361/201732289](https://doi.org/10.1051/0004-6361/201732289)
- Cieza, L. A., Ruíz-Rodríguez, D., Perez, S., et al. 2018, *MNRAS*, 474, 4347, doi: [10.1093/mnras/stx3059](https://doi.org/10.1093/mnras/stx3059)
- Connelley, M. S., & Reipurth, B. 2018, *ApJ*, 861, 145, doi: [10.3847/1538-4357/aaba7b](https://doi.org/10.3847/1538-4357/aaba7b)
- Dent, W. R. F., Matthews, H. E., & Ward-Thompson, D. 1998, *MNRAS*, 301, 1049, doi: [10.1046/j.1365-8711.1998.02091.x](https://doi.org/10.1046/j.1365-8711.1998.02091.x)
- Drozovskaya, M. N., van Dishoeck, E. F., Jørgensen, J. K., et al. 2018, *MNRAS*, 476, 4949, doi: [10.1093/mnras/sty462](https://doi.org/10.1093/mnras/sty462)
- Evans, M. G., Hartquist, T. W., Caselli, P., et al. 2019, *MNRAS*, 483, 1266, doi: [10.1093/mnras/sty2765](https://doi.org/10.1093/mnras/sty2765)
- Evans, M. G., Ilee, J. D., Boley, A. C., et al. 2015, *MNRAS*, 453, 1147, doi: [10.1093/mnras/stv1698](https://doi.org/10.1093/mnras/stv1698)
- Fehér, O., Kóspál, Á., Ábrahám, P., Hogerheijde, M. R., & Brinch, C. 2017, *A&A*, 607, A39, doi: [10.1051/0004-6361/201731446](https://doi.org/10.1051/0004-6361/201731446)
- Fischer, W. J., Hillenbrand, L. A., Herczeg, G. J., et al. 2023, in *Astronomical Society of the Pacific Conference Series*, Vol. 534, *Protostars and Planets VII*, ed. S. Inutsuka, Y. Aikawa, T. Muto, K. Tomida, & M. Tamura, 355, doi: [10.48550/arXiv.2203.11257](https://doi.org/10.48550/arXiv.2203.11257)
- Gaia Collaboration, Brown, A. G. A., Vallenari, A., et al. 2020, *arXiv e-prints*, arXiv:2012.01533. <https://arxiv.org/abs/2012.01533>
- Giannini, T., Schisano, E., Abraham, P., et al. 2024, *arXiv e-prints*, arXiv:2404.01974, doi: [10.48550/arXiv.2404.01974](https://doi.org/10.48550/arXiv.2404.01974)
- Green, J. D., Kraus, A. L., Rizzuto, A. C., et al. 2016, *ApJ*, 830, 29, doi: [10.3847/0004-637X/830/1/29](https://doi.org/10.3847/0004-637X/830/1/29)
- Greene, T. P., Aspin, C., & Reipurth, B. 2008, *AJ*, 135, 1421, doi: [10.1088/0004-6256/135/4/1421](https://doi.org/10.1088/0004-6256/135/4/1421)
- Harris, C. R., Millman, K. J., van der Walt, S. J., et al. 2020, *Nature*, 585, 357, doi: [10.1038/s41586-020-2649-2](https://doi.org/10.1038/s41586-020-2649-2)
- Hartmann, L., Cassen, P., & Kenyon, S. J. 1997, *ApJ*, 475, 770, doi: [10.1086/303547](https://doi.org/10.1086/303547)
- Hartmann, L., & Kenyon, S. J. 1996, *ARA&A*, 34, 207, doi: [10.1146/annurev.astro.34.1.207](https://doi.org/10.1146/annurev.astro.34.1.207)
- Herbig, G. H. 1977, *ApJ*, 217, 693, doi: [10.1086/155615](https://doi.org/10.1086/155615)
- Hunter, J. D. 2007, *Computing in Science & Engineering*, 9, 90, doi: [10.1109/MCSE.2007.55](https://doi.org/10.1109/MCSE.2007.55)
- Jørgensen, J. K., Bourke, T. L., Myers, P. C., et al. 2007, *ApJ*, 659, 479, doi: [10.1086/512230](https://doi.org/10.1086/512230)
- Jørgensen, J. K., Müller, H. S. P., Calcutt, H., et al. 2018, *A&A*, 620, A170, doi: [10.1051/0004-6361/201731667](https://doi.org/10.1051/0004-6361/201731667)
- Kuhn, M. A., & Hillenbrand, L. A. 2019, *ApJ*, 883, 117, doi: [10.3847/1538-4357/ab3a3f](https://doi.org/10.3847/1538-4357/ab3a3f)
- Law, C. J., Booth, A. S., & Öberg, K. I. 2023, *ApJL*, 952, L19, doi: [10.3847/2041-8213/acdfd0](https://doi.org/10.3847/2041-8213/acdfd0)
- Le Gal, R., Öberg, K. I., Huang, J., et al. 2020, *ApJ*, 898, 131, doi: [10.3847/1538-4357/ab9ebf](https://doi.org/10.3847/1538-4357/ab9ebf)
- Le Roy, L., Altwegg, K., Balsiger, H., et al. 2015, *A&A*, 583, A1, doi: [10.1051/0004-6361/201526450](https://doi.org/10.1051/0004-6361/201526450)
- Lee, J.-E., Lee, S., Baek, G., et al. 2019, *Nature Astronomy*, 3, 314, doi: [10.1038/s41550-018-0680-0](https://doi.org/10.1038/s41550-018-0680-0)
- Lee, J.-E., Kim, C.-H., Lee, S., et al. 2024, *ApJ*, 966, 119, doi: [10.3847/1538-4357/ad3106](https://doi.org/10.3847/1538-4357/ad3106)
- Liu, H. B., Galván-Madrid, R., Vorobyov, E. I., et al. 2016, *ApJL*, 816, L29, doi: [10.3847/2041-8205/816/2/L29](https://doi.org/10.3847/2041-8205/816/2/L29)
- Manigand, S., Jørgensen, J. K., Calcutt, H., et al. 2020, *A&A*, 635, A48, doi: [10.1051/0004-6361/201936299](https://doi.org/10.1051/0004-6361/201936299)
- Marchand, P., Coutens, A., Scigliuto, J., et al. 2024, *arXiv e-prints*, arXiv:2405.08517, doi: [10.48550/arXiv.2405.08517](https://doi.org/10.48550/arXiv.2405.08517)
- McClure, M. K., Rocha, W. R. M., Pontoppidan, K. M., et al. 2023, *Nature Astronomy*, 7, 431, doi: [10.1038/s41550-022-01875-w](https://doi.org/10.1038/s41550-022-01875-w)
- Ohashi, N., Tobin, J. J., Jørgensen, J. K., et al. 2023, *ApJ*, 951, 8, doi: [10.3847/1538-4357/acd384](https://doi.org/10.3847/1538-4357/acd384)
- Pegues, J., Öberg, K. I., Bergner, J. B., et al. 2020, *ApJ*, 890, 142, doi: [10.3847/1538-4357/ab64d9](https://doi.org/10.3847/1538-4357/ab64d9)
- Persson, M. V., Jørgensen, J. K., & van Dishoeck, E. F. 2013, *A&A*, 549, L3, doi: [10.1051/0004-6361/201220638](https://doi.org/10.1051/0004-6361/201220638)
- Pickering, E. C. 1890, *The Observatory*, 13, 80
- Principe, D. A., Cieza, L., Hales, A., et al. 2018, *MNRAS*, 473, 879, doi: [10.1093/mnras/stx2320](https://doi.org/10.1093/mnras/stx2320)
- Rivière-Marichalar, P., Fuente, A., Le Gal, R., et al. 2020, *A&A*, 642, A32, doi: [10.1051/0004-6361/202038549](https://doi.org/10.1051/0004-6361/202038549)
- Rubin, M., Altwegg, K., Balsiger, H., et al. 2019, *MNRAS*, 489, 594, doi: [10.1093/mnras/stz2086](https://doi.org/10.1093/mnras/stz2086)

- Szabó, Z. M., Kóspál, Á., Ábrahám, P., et al. 2021, *ApJ*, 917, 80, doi: [10.3847/1538-4357/ac04b3](https://doi.org/10.3847/1538-4357/ac04b3)
- . 2022, *ApJ*, 936, 64, doi: [10.3847/1538-4357/ac82f5](https://doi.org/10.3847/1538-4357/ac82f5)
- Tobin, J. J., van't Hoff, M. L. R., Leemker, M., et al. 2023, *Nature*, 615, 227, doi: [10.1038/s41586-022-05676-z](https://doi.org/10.1038/s41586-022-05676-z)
- Tran, V., De, K., & Hillenbrand, L. 2024, *MNRAS*, 530, 2076, doi: [10.1093/mnras/stae953](https://doi.org/10.1093/mnras/stae953)
- van 't Hoff, M. L. R., Tobin, J. J., Trapman, L., et al. 2018, *ApJL*, 864, L23, doi: [10.3847/2041-8213/aadb8a](https://doi.org/10.3847/2041-8213/aadb8a)
- van't Hoff, M. L. R., Bergin, E. A., Riley, P., et al. 2024, *ApJ*, 970, 138, doi: [10.3847/1538-4357/ad4be4](https://doi.org/10.3847/1538-4357/ad4be4)
- Vastel, C., Bottinelli, S., Caux, E., Glorian, J. M., & Boiziot, M. 2015, in *SF2A-2015: Proceedings of the Annual meeting of the French Society of Astronomy and Astrophysics*, 313–316
- Visser, R., Bergin, E. A., & Jørgensen, J. K. 2015, *A&A*, 577, A102, doi: [10.1051/0004-6361/201425365](https://doi.org/10.1051/0004-6361/201425365)
- Vorobyov, E. I., & Basu, S. 2006, *ApJ*, 650, 956, doi: [10.1086/507320](https://doi.org/10.1086/507320)
- Vorobyov, E. I., Zakhochay, O. V., & Dunham, M. M. 2013, *MNRAS*, 433, 3256, doi: [10.1093/mnras/stt970](https://doi.org/10.1093/mnras/stt970)
- Yamato, Y., Notsu, S., Aikawa, Y., et al. 2024, *AJ*, 167, 66, doi: [10.3847/1538-3881/ad11d9](https://doi.org/10.3847/1538-3881/ad11d9)
- Zhu, Z., Hartmann, L., & Gammie, C. 2010, *ApJ*, 713, 1143, doi: [10.1088/0004-637X/713/2/1143](https://doi.org/10.1088/0004-637X/713/2/1143)